Article

New Tetragonal ReGa$_5$(M) (M = Sn, Pb, Bi) Single Crystals Grown from Delicate Electrons Changing

Madalynn Marshall [1], Karolina Górnicka [2], Ranuri S. Dissanayaka Mudiyanselage [1], Tomasz Klimczuk [2] and Weiwei Xie [1],*

[1] Department of Chemistry, Louisiana State University, Baton Rouge, LA 70803, USA; mmars44@lsu.edu (M.M.); rdissa1@lsu.edu (R.S.D.M.)
[2] Faculty of Applied Physics and Mathematics, Gdansk University of Technology, Narutowicza 11/12, 80-233 Gdansk, Poland; karolinagornicka@wp.pl (K.G.); tomasz.klimczuk@pg.edu.pl (T.K.)
* Correspondence: weiweix@lsu.edu

check for
updates

Abstract: Single crystals of the new Ga-rich phases ReGa$_{\sim5}$(Sn), ReGa$_{\sim5}$(Pb) and ReGa$_{\sim5}$(Bi) were successfully obtained from the flux method. The new tetragonal phases crystallize in the space group *P4/mnc* (No. 128) with vertex-sharing capped Re$_2$@Ga$_{14}$ oblong chains. Vacancies were discovered on the Ga4 and Ga5 sites, which can be understood as the direct inclusion of elemental Sn, Pb and Bi into the structure. Heat capacity measurements were performed on all three compounds resulting in a small anomaly which resembles the superconductivity transition temperature from the impurity ReGa$_5$ phase. The three compounds were not superconducting above 1.85 K. Subsequently, electronic structure calculations revealed a high density of states around the Fermi level, as well as non-bonding interactions that likely indicate the stability of these new phases.

Keywords: endohedral; gallide; clusters

1. Introduction

Endohedral gallium cluster phases are a chemical family that has been sought after for their various electronic properties arising from the interesting cluster chemistry associated with gallium's moderate electronegativity [1,2]. However, because of overly large anionicity, isolated Ga clusters will very rarely form. This leads to a significant interplay between Ga cluster-cluster interactions, i.e., exo-bond formations and the stability of the electronic structures. While moving across the periodic table, a spectrum of diverse Ga cluster phases can be observed. Beginning with electropositive alkali metals (A), A$_m$Ga$_n$ compounds most readily form electron precise Zintl phases as a result of the large electronegativity difference, making a promising candidate for thermoelectric materials [3–5]. In this sense, electrons will be transferred from the alkali metals to Ga$_n$ clusters to satisfy its valence electron requirement. Many of these compounds will form deltahedral clusters, as in borane chemistry, and have skeletal electron counts which will typically follow Wade's rules [6].

Decreasing the electronegativity difference and transitioning towards actinides and lanthanides (R), a significant reduction in the band gap is observed and, in some cases is completely diminished, resulting in metallic behavior. In search of stability, R$_m$Ga$_n$ clusters often distort from ideal deltahedral symmetries and form exo-bonds [7]. The addition of transition metals into R$_m$Ga$_n$ clusters can reduce the cluster charge and has led to various intriguing materials such as the unconventional superconductor PuCoGa$_5$ [8]. Finally, coming to the transition metal (T) gallide clusters, the ionic behavior becomes more obscure as a result of the similar electronegativities between Ga and transition metals. In this region, the relationship between electron counts and cluster formation with regards to the superconductivity transition temperature, unfolds. Currently, the only known T$_m$Ga$_n$ superconductors

are low-temperature superconductors, making them potential materials for producing high magnetic fields at low temperatures. This can be observed in the superconductors Mo_8Ga_{41} and Mo_6Ga_{31}—as the electron counts decrease, the T_c increases and the clusters form vertex-sharing interactions rather than edge-sharing [9]. $MnGa_{4.96}$ is another Ga-rich cluster which crystallizes into a tetragonal unit cell with capped face sharing $Mn@Ga_8$ clusters and correspondingly exhibits no superconductivity [10]. Therefore, the stoichiometry and valence electrons from the transition metal of endohedral gallide clusters play a critical role in the exo-bond formations, i.e., electron-rich clusters prefer edge-sharing while electron-poor ones prefer vertex-sharing clusters, which as a result, directly affects the T_c. Considering the significant decrease in T_c from Rh_2Ga_9 to Ir_2Ga_9, and contradictorily the increase in T_c from Cr-Ga to Mo-Ga clusters, the transition of T_c across T_mGa_n clusters can be further analyzed [11–13].

Narrowing the spectrum down to the $5d$ transition metal gallide clusters below Mn in group 7, we sought to further investigate the recently discovered $ReGa_5$ superconductor with a T_c of ~2.3 K and vertex sharing $Re@Ga_9$ clusters [14]. Proceeding to understand the structural characteristics and electron counts of endohedral Ga clusters on superconductivity and further exploring new Re-Ga phases, we successfully discovered three new compounds $ReGa_{\sim5}(Sn)$, $ReGa_{\sim5}(Pb)$ and $ReGa_{\sim5}(Bi)$. Reported here are the heat capacity measurements along with the crystal and electronic structure characterizations. No superconductivity was found for $ReGa_{\sim5}(Sn)$, $ReGa_{\sim5}(Pb)$ and $ReGa_{\sim5}(Bi)$ down to 1.85 K.

2. Experimental Section

Synthesis. The new compounds $ReGa_{\sim5}(Sn)$, $ReGa_{\sim5}(Pb)$ and $ReGa_{\sim5}(Bi)$ were synthesized via flux method using Ga as the self-flux. Elements used include tin granules (99.9%, BTC), lead shots (99.999%, BTC), bismuth chunks (99.999%, lump, Alfa Aesar), gallium ingot (99.99% (metals basis), Alfa Aesar) and rhenium powder (−325 mesh, 99.99% (metals basis), Alfa Aesar). The three reactions were prepared with sample sizes of ~1.5–2.0 g and loading compositions of $ReSnGa_{48}$, $RePb_5Ga_{25}$ and $ReBi_5Ga_{25}$. Each sample was placed in an alumina crucible then inside a silica tube. Quartz glass pieces and quartz wool were packed on top of the crucible as the filter. The silica tube was subsequently evacuated ($<10^{-5}$ Torr) and sealed. Samples were heated to 950 °C at a rate of 200 °C/hr and annealed there for 24hr then slow cooled at a rate of 10 °C/hr for $ReGa_{\sim5}(Sn)$ and 4 °C/hr for $ReGa_{\sim5}(Pb)$ and $ReGa_{\sim5}(Bi)$ to 600 °C at which the samples were centrifuged. Excess Ga flux was removed using ~2 M HCl. All products are found to be stable in air and moisture.

Phase Analysis. For each $ReGa_{\sim5}(Sn)$, $ReGa_{\sim5}(Pb)$ and $ReGa_{\sim5}(Bi)$ sample the phase was identified and purity verified through a Rigaku MiniFlex 600 powder X-ray diffractometer using Cu Kα radiation ($\lambda_{K\alpha}$ = 1.5406 Å, Ge monochromator) [15]. A scan speed of 1.25°/min and step of 0.005° were used over a Bragg angle (2θ) ranging from 5 to 90° for $ReGa_{\sim5}(Pb)$ and $ReGa_{\sim5}(Bi)$. For $ReGa_{\sim5}(Sn)$ a scan speed of 0.6°/min and step of 0.005° were used over a Bragg angle (2θ) ranging from 10 to 90°. Full Proof software was used to analyze the phase identification and lattice parameters of the experimental and theoretical powder patterns for $ReGa_{\sim5}(Sn)$, $ReGa_{\sim5}(Pb)$ and $ReGa_{\sim5}(Bi)$ and the experimental powder patterns for the impurity phases obtained from ICSD [16].

Structure Determination. Single crystals from $ReGa_{\sim5}(Sn)$, $ReGa_{\sim5}(Pb)$ and $ReGa_{\sim5}(Bi)$ were picked to perform a structural analysis using a Bruker Apex II diffractometer equipped with Mo radiation ($\lambda_{K\alpha}$ = 0.71073 Å). Scattering intensity data were collected at room temperature with 0.5° per scan in ω and an exposure time of 10s per frame. The crystal structure was solved using a SHELXTL package with direct methods and full-matrix least-squares on F^2 model [17,18].

Scanning Electron Microscopy. A FEI Quanta 3D Field Emission Gun (FEG) Focused Ion Beam (FIB)/Scanning Electron Microscope (SEM) and Energy Dispersive X-ray Spectroscopy (EDX) were utilized with the analysis of chemical stoichiometry. For each sample, multiple areas were selected for spectrum collection with a 20kV accelerating voltage and 100 seconds of scanning time.

Physical Property Measurements. Heat capacity measurements were carried out using the two-τ time- relaxation method in a Physical Property Measurement System (PPMS). The data was collected

between 1.85 and 300 K. The sample was mounted to the measuring stage using Apiezon N grease to ensure good thermal contact.

***Tight-Binding, Linear Muffin-Tin Orbital-Atomic Sphere Approximation* (TB-LMTO-ASA)** [19]. The TB-LMTO-ASA program with Stuttgart code was utilized to calculate the density of states (DOS) and Orbital Hamiltonian Population (COHP) curves of a hypothetically ordered "ReGa$_{4.5}$" [20,21]. The convergence criterion was set to 0.05 meV. The Muffin-Tin radius (RMT) for each element includes: 0.995 Å for Re1; 1.40 Å for Ga2; 1.88 Å for Ga3; 0.83 Å for Ga4. The band structure and DOS were both calculated with a $4 \times 4 \times 2$ k-point in the Brillouin zone [22,23].

3. Results and Discussions

Phase Analysis. As a result of increasing the valence electron count from the orthorhombic ReGa$_5$, three new tetragonal phases ReGa$_{\sim 5}$(Sn), ReGa$_{\sim 5}$(Pb) and ReGa$_{\sim 5}$(Bi) were revealed. Unreacted Re was present in all of the three compounds ranging from 5–15% as well as ReGa$_5$ from 0.1–39%, based on the HighScore Plus software. Unreacted Pb and Bi were also found in both ReGa$_{\sim 5}$(Pb) and ReGa$_{\sim 5}$ (Bi) by approximately 3 and 7%, respectively. A comparison of the three powder patterns, as well as images of the single crystals, are shown in Figure 1. Individual refined powder patterns of the three phases can be found in Figure S1 (Supplementary Materials) of the Supporting Information. To confirm the chemical composition and stoichiometry SEM-EDS was utilized. The determined chemical formulas are Re$_{1.0(3)}$Ga$_{5.0(2)}$Sn$_{0.1(8)}$, Re$_{1.0(2)}$Ga$_{5.0(2)}$Pb$_{0.1(5)}$ and Re$_{1.0(2)}$Ga$_{5.0(2)}$Bi$_{0.2(4)}$. A complete table of the SEM-EDS data is shown in Table S2 in the Supporting Information.
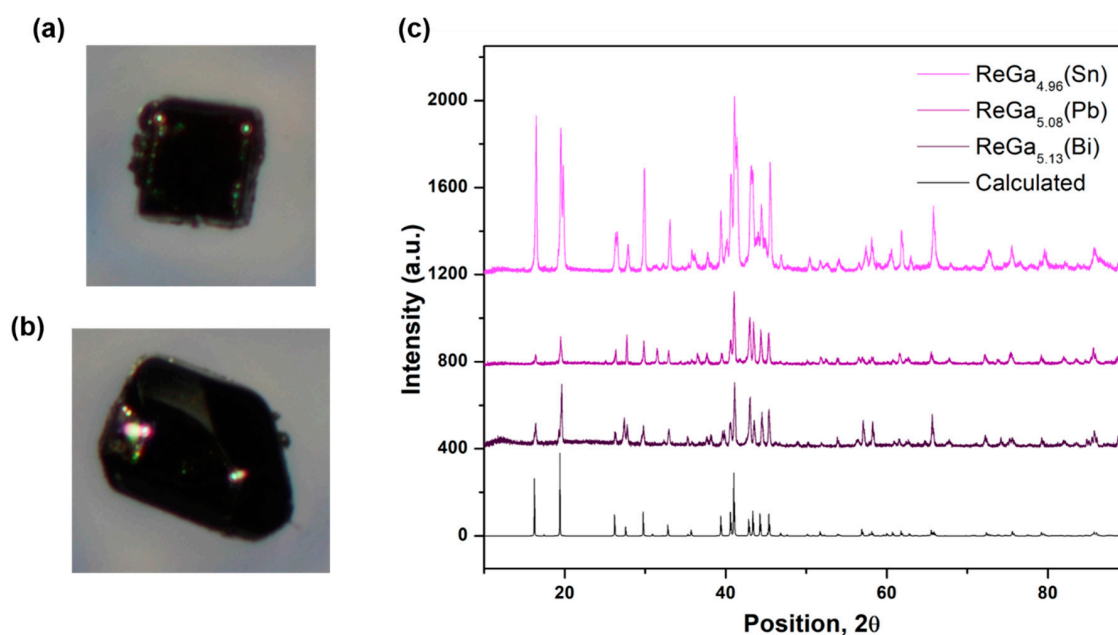

Figure 1. (**a**,**b**) Pictures of the ReGa$_{\sim 5}$(Sn) single crystals. (**c**) Powder XRD patterns for ReGa$_{\sim 5}$(Sn), ReGa$_{\sim 5}$(Pb) and ReGa$_{\sim 5}$(Bi).

Crystal Structure. Single crystal X-ray diffraction was utilized to further understand the effect of atomic size and electron counts on the stability of Ga-rich phases. As a result of the increase in valence electron counts induced from the elements Sn, Pb and Bi, a tetragonal structure with space group *P4/mnc* (No. 128) was formed. A table of the single crystal refinement data as well as atomic coordinates and equivalent isotropic displacement parameters are given in Tables 1 and 2. The three new phases ReGa$_{\sim 5}$(Sn), ReGa$_{\sim 5}$(Pb) and ReGa$_{\sim 5}$(Bi) consist of two face-sharing square antiprismatic Re@Ga$_8$ polyhedra capped by four Ga atoms, or five Ga atoms when considering ReGa$_{\sim 5}$(Sn), on the remaining free square faces. Consequently, these clusters form networks of vertex sharing capped Re$_2$@Ga$_{14}$

oblong chains, similar to $MnGa_{4.96}$. The $Re@Ga_8$ clusters in $ReGa_{\sim5}(Sn)$, $ReGa_{\sim5}(Pb)$ and $ReGa_{\sim5}(Bi)$ resemble the geometry of the $Re@Ga_9$ endohedral clusters found in the $ReGa_5$ orthorhombic structure, however, in this case, the polyhedra are more than singly capped. Conversely, the $Re@Ga_9$ clusters in $ReGa_5$ are vertex sharing, while $ReGa_{\sim5}(Sn)$, $ReGa_{\sim5}(Pb)$ and $ReGa_{\sim5}(Bi)$ not only have vertex sharing but also face sharing polyhedra, which resultantly produces the capped $Re_2@Ga_{14}$ oblong chains. As seen in the decrease in T_c from the superconductor Mo_8Ga_{41} to Mo_6Ga_{31} the exo-bond formation, as well as the additional electron counts, may be a key factor causing the loss of superconductivity in $ReGa_{\sim5}(Sn)$, $ReGa_{\sim5}(Pb)$ and $ReGa_{\sim5}(Bi)$. Initially, atomic vacancies were tested and revealed vacancies on the Ga4 and Ga5 sites. The Ga4 site vacancies were found to vary significantly depending on the electron count. After further inspection of the change in atomic distances with varying electron count, it was found that the Re-Ga4 distance experiences the most significant change. A table of atomic distances for each new phase is given in Table 3. This occurrence may have been understood by the $Re@Ga_8$ polyhedra undergoing stretching and compression due to the various applied chemical pressures. However, the atomic distances in the $Re@Ga_8$ polyhedra appear to remain relatively consistent. The changes in distance experienced by Re-Ga4 resulted from the vacancies on the Ga4 site. As the vacancies decrease, the Ga4 site merges two atoms into one and the Re-Ga4 distance increases. This occurs as the structure changes from Sn to Bi to Pb, where $ReGa_{\sim5}(Sn)$ and $ReGa_{\sim5}(Bi)$ have Ga4 on the 4e site while $ReGa_{\sim5}(Pb)$ has Ga4 on the 2a site. As a result, the Ga4 and Ga5 vacancies can be realized as Sn, Pb and Bi giving a mixture of Ga and Sn, Pb or Bi on the Ga4 and Ga5 sites, as shown in Figure 2d. Therefore, considering both the atomic size and electron count of Sn, Pb and Bi the changing Ga4 vacancies and Re-Ga4 distance can be well understood. Taking into account that the most significant changes are resulting from the Re-Ga4 and the Ga5-Ga5 distances (diagonally along the *b* axis) then both can be recognized as contributing factors to the change in structure between the three compounds. The four Ga5 atoms that sit on either side of the Ga4 site seem to open and compress, in sync with the Ga5 occupancies as the Ga4 atomic vacancy and site location changes, subsequently pushing Ga4 from the 4e to the 2a site. This then increases the Re-Ga4 distance as the structures transition from $ReGa_{\sim5}(Sn)$ to $ReGa_{\sim5}(Bi)$ to $ReGa_{\sim5}(Pb)$.

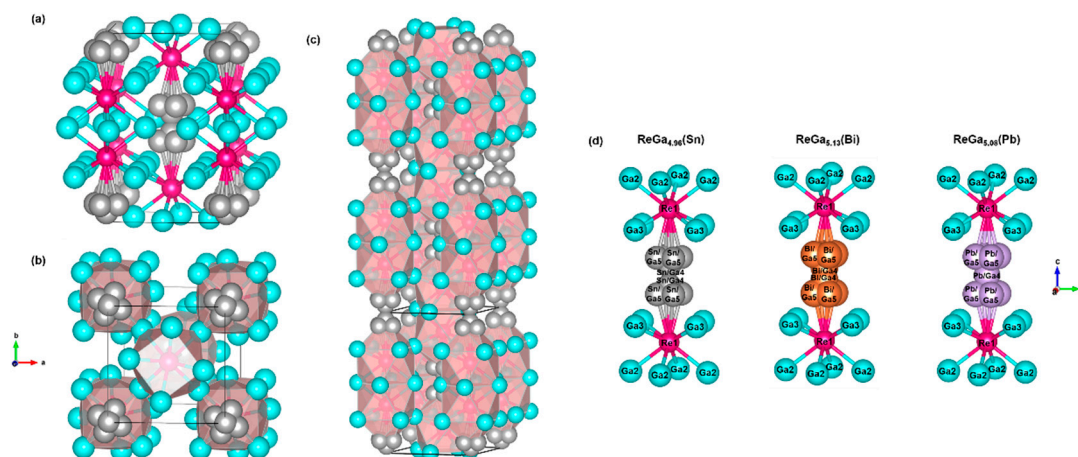**Figure 2.** Shown in this image is the structure of $ReGa_{\sim5}(Sn)$ (Re, purple; Ga, blue; Sn, grey) displaying a unit cell of the capped square antiprismatic $Re@Ga8$ polyhedra projection on the (**a**) *bc* plane and (**b**) *ab* plane. (**c**) Crystal structure of $ReGa_{\sim5}(Sn)$ showing the networks of capped $Re_2@Ga_{14}$ oblong chains. (**d**) Image comparing the capped $Re_2@Ga_{14}$ oblong chain of $ReGa_{\sim5}(Sn)$, $ReGa_{\sim5}(Pb)$ (Pb, purple) and $ReGa_{\sim5}(Bi)$ (Bi, orange).

Table 1. Single crystal refinement data for $ReGa_{4.96}(Sn)$, $ReGa_{5.08}(Pb)$ and $ReGa_{5.13}(Bi)$.

Refined Formula	$ReGa_{4.96(9)}(Sn)$	$ReGa_{5.08(5)}(Pb)$	$ReGa_{5.13(5)}(Bi)$
FW (g/mol)	532.19	540.55	543.86
Space group; Z	*P 4/m n c*; 4	*P 4/m n c*; 4	*P 4/m n c*; 4
a (Å)	6.4680(9)	6.4830(13)	6.474(2)
c (Å)	10.166(2)	10.229(2)	10.213(4)
V (Å³)	425.29(15)	429.9(2)	428.0(3)
Extinction Coefficient	0.0017(4)	0.0037(3)	0.0044(3)
θ range (°)	3.734–33.135	3.721–33.166	3.726–33.240
No. reflections; R_{int}	5007; 0.0646	5731; 0.0700	5798; 0.1039
No. independent reflections	429	436	438
No. parameters	30	29	30
R_1; ωR_2 ($I > 2\delta(I)$)	0.0397; 0.0932	0.0284; 0.0552	0.0263; 0.0464
Goodness of fit	1.311	1.197	0.999
Diffraction peak and hole (e⁻/Å³)	2.713; −2.981	1.572; −2.359	1.822; −1.863

Table 2. Atomic coordinates and equivalent isotropic displacement parameters for $ReGa_{4.96}(Sn)$, $ReGa_{5.08}(Pb)$ and $ReGa_{5.13}(Bi)$ (U_{eq} is defined as one-third of the trace of the orthogonalized U_{ij} tensor (Å²)).

Atom	Wyck.	x	y	z	Occ.	U_{eq}
			$ReGa_{4.96(9)}(Sn)$			
Re	4e	0	0	0.3451(1)	1	0.008(1)
Ga2	8h	0.4535(3)	0.1808(3)	0	1	0.016(1)
Ga3	8g	0.7431(3)	0.2431(3)	$\frac{1}{4}$	1	0.045(1)
Ga4	4e	0	0	0.051(3)	0.18(3)	0.021(8)
Ga5	16i	0.0426(18)	0.096(2)	0.0947(8)	0.20(1)	0.028(4)
			$ReGa_{5.08(5)}(Pb)$			
Re	4e	0	0	0.3453(1)	1	0.007(1)
Ga2	8h	0.4622(2)	0.1816(2)	0	1	0.016(1)
Ga3	8g	0.7462(2)	0.2462(2)	$\frac{1}{4}$	1	0.040(1)
Ga4	2a	0	0	0	0.75(1)	0.022(1)
Ga5	16i	0.0389(11)	0.0883(19)	0.0970(5)	0.18(1)	0.024(2)
			$ReGa_{5.13(5)}(Bi)$			
Re	4e	0	0	0.3451(1)	1	0.006(1)
Ga2	8h	0.4692(1)	0.1821(1)	0	1	0.018(1)
Ga3	8g	0.7467(1)	0.2467(1)	$\frac{1}{4}$	1	0.033(1)
Ga4	4e	0	0	0.0318(3)	0.62(1)	0.012(1)
Ga5	16i	0.039(2)	0.079(5)	0.1001(6)	0.13(1)	0.027(3)

Table 3. List of atomic distances for $ReGa_{4.96}(Sn)$, $ReGa_{5.08}(Pb)$ and $ReGa_{5.13}(Bi)$.

	$ReGa_{4.96}(Sn)$	
Atom1	**Atom2**	**Distances (Å)**
Re	Ga2	2.614(2)
Re	Ga3	2.484(2)
Re	Ga4	2.99(4)
Re	Ga5	2.635(9)
Ga5	Ga5	1.36(3) (diagonally along the *b* axis)

Table 3. *Cont.*

ReGa$_{5.08}$(Pb)		
Atom1	**Atom2**	**Distances (Å)**
Re	Ga2	2.612(1)
Re	Ga3	2.491(1)
Re	Ga4	3.5322(6)
Re	Ga5	2.616(6)
Ga5	Ga5	1.25(1) (diagonally along the b axis)
ReGa$_{5.13}$(Bi)		
Atom1	**Atom2**	**Distances (Å)**
Re	Ga2	2.604(1)
Re	Ga3	2.487(1)
Re	Ga4	3.200(4)
Re	Ga5	2.566(8)
Ga5	Ga5	1.14(4) (diagonally along the *b* axis)

Physical Properties. To evaluate the impact of chemical pressure on superconductivity, specific heat measurements were carried out. Figure 3a,c,e show the specific heat data plotted as, C_P/T versus T^2, and Figure 3b,d,f display C_P versus T for ReGa$_{\sim5}$(Sn), ReGa$_{\sim5}$(Pb) and ReGa$_{\sim5}$(Bi), respectively. The low-temperature experimental data (obtained under field of 0.3 T) were fitted using $C_p/T = \gamma + \beta T^2$, where the first and second terms are attributed to the electronic (C_{el}) and lattice contributions (C_{ph}) to the specific heat, respectively. The fit, represented by the red solid line (see Figure 3a,c,e), gives the Sommerfeld coefficient, γ, 4.0(1), 3.4(1), and 3.5(2) mJ mol^{-1} K^{-2} and β equals to 0.39(2), 0.55(1) and 0.84(3) mJ mol^{-1} K^{-4} for ReGa$_{\sim5}$(Sn), ReGa$_{\sim5}$(Pb) and ReGa$_{\sim5}$(Bi), respectively. Furthermore, the Debye temperature Θ_D can be determined using the simple Debye model: $\Theta_D = \left(\frac{12\pi^4}{5\beta}nR\right)^{1/3}$, where R = 8.31 J mol^{-1}K^{-1}. The calculated Debye temperature Θ_D is 309(4), 275(1) and 239(1) K for compounds with elemental Sn, Pb and Bi, respectively. The obtained values of the Sommerfeld coefficient and Debye temperature are significantly lower when compared with ReGa$_5$ (γ = 4.68(7) mJ mol^{-1} K^{-2} and Θ_D = 314(2)K). A small anomaly at around 2.2 K, is observed for each phase in the specific heat data measured under zero field, that resembles the critical superconducting temperature of ReGa$_5$ (not shown here). This is consistent with the high concentration of ReGa$_5$ present in each compound. Thus, we conclude that no phase transition was observed for ReGa$_{\sim5}$(Sn), ReGa$_{\sim5}$(Pb) and ReGa$_{\sim5}$(Bi), indicating that the effect of the valence electron counts on the ReGa$_5$ system resulted not only in a change of the crystal structure but also a loss of superconductivity. The whole temperature range $C_p(T)$, see Figure 3b,d,f, shows a typical behavior and at high temperature, C_p approaches the expected Dulong–Petit value (3nR ≈ 150 J mol^{-1} K^{-1}), where n is the number of atoms per formula unit (n = 6) and R is the gas constant (R = 8.31 J mol^{-1} K^{-1}).
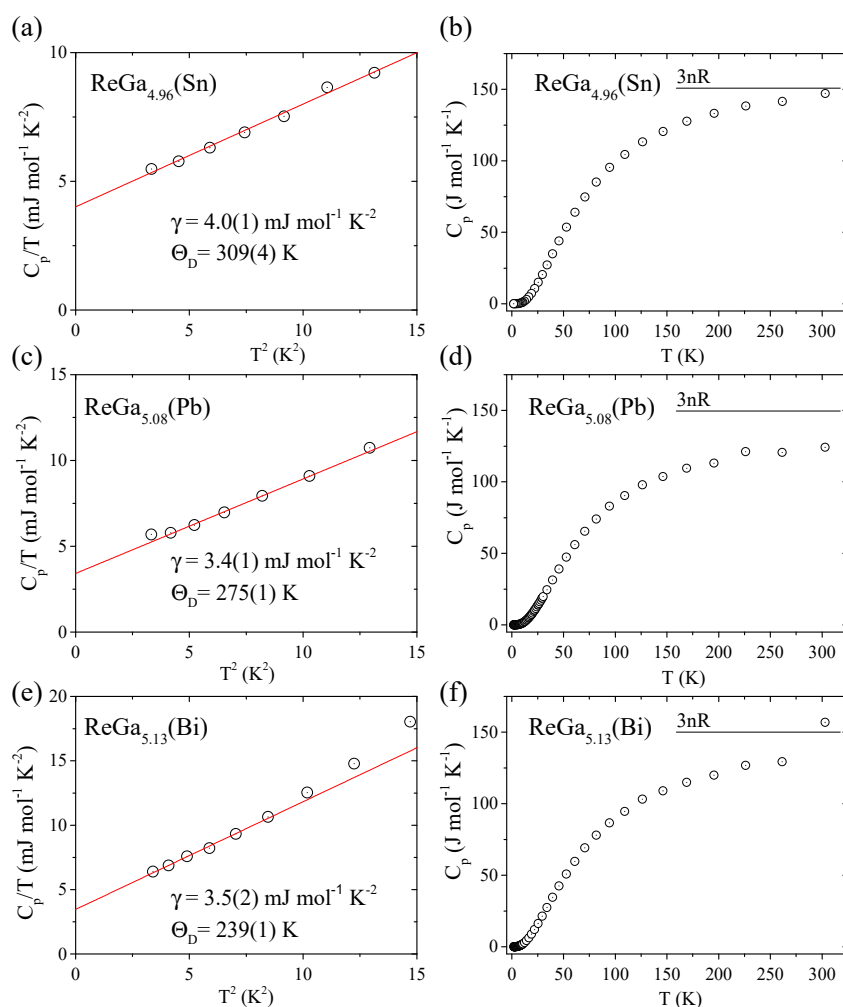
Figure 3. (**a,c,e**) Heat capacity ($C_P(T)/T \sim T^2$) range 1.85 to 300 K for ReGa$_{\sim5}$(Sn), ReGa$_{\sim5}$(Pb) and ReGa$_{\sim5}$(Bi) to obtain the Sommerfeld parameter (γ) and Debye temperature (θ_D). (**b,d,f**) Heat capacity ($C_P(T) \sim T$) range 1.85 to 300 K for ReGa$_{\sim5}$(Sn), ReGa$_{\sim5}$(Pb) and ReGa$_{\sim5}$(Bi).

Electronic Structure. To evaluate the influence of the electronic structure on ReGa$_{\sim5}$(Sn), ReGa$_{\sim5}$(Pb) and ReGa$_{\sim5}$(Bi), TB-LMTO-ASA calculations were performed to analyze the density of states (DOS), Crystal Orbital Hamiltonian Population (-COHP) curves and band structures. Due to the Ga vacancies and close proximity with regards to other atoms, a hypothetical "ReGa$_{4.5}$" was utilized to calculate the electronic structure, these plots are shown in Figure 4a–c. Based on the stoichiometry of Sn, Pb and Bi determined from the SEM/EDS data, the electron counts of ReGa$_{4.96}$Sn$_{0.1}$, ReGa$_{5.08}$Pb$_{0.1}$ and ReGa$_{5.13}$Bi$_{0.2}$ were calculated to be 22.28, 22.64 and 23.39 valence electrons (VE) per Re, respectively. The Fermi energy level is indicated for each compound in Figure 4. As seen with ReGa$_5$ and other endohedral gallide cluster superconductors, the Fermi energy level is located in a pseudo gap in the DOS, which is thought to play a role in the structural stability [24]. However, no von Hove singularities are found in the electronic structure of ReGa$_{4.96}$(Sn), ReGa$_{5.08}$(Pb) and ReGa$_{5.13}$(Bi) around the Fermi level [25]. Consequently, this could be a key factor in the loss of superconductivity in these gallide clusters. This is consistent with the band structure calculation, Figure 4c, which indicates metallic behavior and shows no sign of flat bands near the Fermi energy. The DOS at the Fermi energy increases from ReGa$_{5.08}$(Pb) to ReGa$_{5.13}$(Bi) to ReGa$_{4.96}$(Sn) suggesting the stability of the structures may come from the degree of Ga4 vacancies. -COHP curves, shown in Figure 4b, were calculated to analyze the interactions between Re and Ga in ReGa$_{\sim5}$(Sn), ReGa$_{\sim5}$(Pb) and ReGa$_{\sim5}$(Bi). The -COHP shows the Fermi levels tend to move from strong antibonding interactions to the non-bonding interactions. This

could be strongly related to the structural stability of these distorted phases and a major influence on the lack of superconductivity.
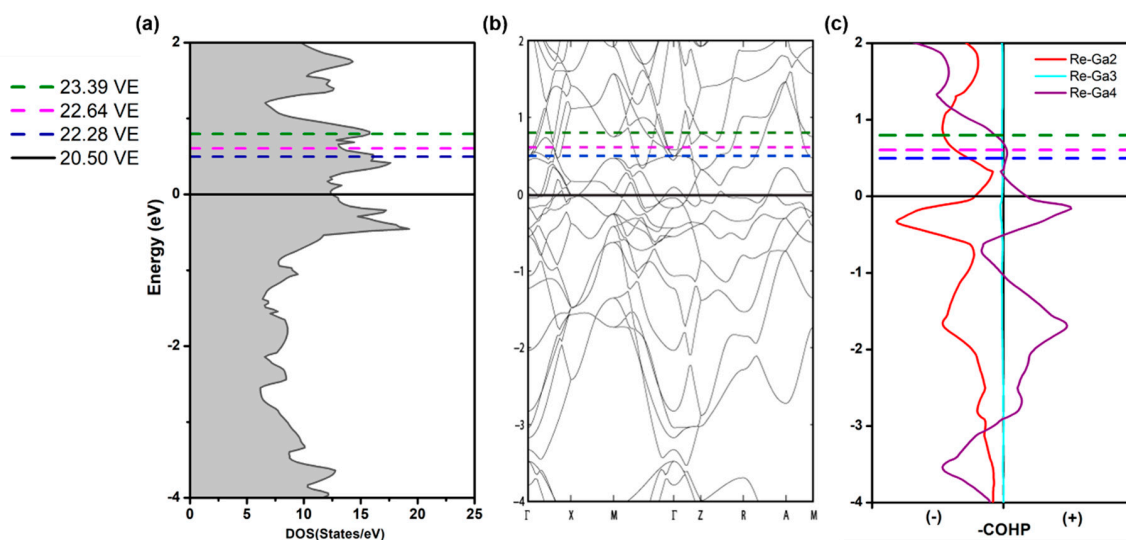

Figure 4. Electronic structure calculations with a black solid line indicating the Fermi level for theoretical $ReGa_{4.5}$ and a dashed blue, pink and green line indicating the Fermi energy level for $ReGa_{4.96}(Sn)$, $ReGa_{5.08}(Pb)$ and $ReGa_{5.13}(Bi)$, respectively, for the (**a**) density of states (DOS) curves, obtained from Local-Density Approximation (LDA), (**b**) band structure and (**c**) Orbital Hamiltonian Population Curves (COHP), for Re-Ga interactions.

4. Conclusions

The understanding of Ga-rich T_mGa_n endohedral clusters was further assessed through three new phases: $ReGa_{\sim 5}(Sn)$; $ReGa_{\sim 5}(Pb)$ and $ReGa_{\sim 5}(Bi)$ presented here. The crystal structure characterization reveals that the new phases crystallize in a tetragonal unit cell resembling that of $MnGa_{4.96}$. The electron-rich new Re-Ga phases produced edge-sharing polyhedra, further confirming the exo-bond formations between electron-rich and poor gallide clusters. Heat capacity measurements were performed, and no superconductivity was found down to 1.85 K, only a small anomaly associated with the $ReGa_5$ superconductivity transition temperature. The Sommerfeld and Debye temperatures are significantly lower than $ReGa_5$. Electronic structure calculations offered additional insight into the structural stability. Conclusively, the non-bonding character and absence of a pseudo gap and at the Fermi energy level along with the capped face sharing square antiprismatic $Re@Ga_8$ polyhedra likely have a direct impact on the structural stability and loss of superconductivity in these Re-Ga clusters. These non-superconducting compounds may be useful for other potential applications.

Author Contributions: Conceptualization, M.M. and W.X.; methodology, M.M. K.G., R.S.D.M.; writing—original draft preparation, M.M.; writing—review and editing, W.X., K.G., R.S.D.M., T.K.; supervision, W.X.

Conflicts of Interest: The authors declare no conflict of interest.

References

1. Poole, C.K.; Farach, H.A.; Creswick, R.J. *Handbook of Superconductivity*; Elsevier: Amsterdam, The Netherlands, 1999.

2. Henning, R.W.; Corbett, J.D. Formation of Isolated Nickel-Centered Gallium Clusters in $Na_{10}Ga_{10}Ni$ and a 2-D Network of Gallium Octahedra in K_2Ga_3. *Inorg. Chem.* **1999**, *38*, 3883–3888. [CrossRef]

3. Belin, C.; Tillard-Charbonnel, M. Frameworks of clusters in alkali metal-gallium phases: Structure, bonding and properties. *Prog. Solid State Chem.* **1993**, *22*, 59–109. [CrossRef]

4. Henning, R.W.; Corbett, J.D. Cs_8Ga_{11}, a New Isolated Cluster in a Binary Gallium Compound. A Family of Valence Analogues $A_8Tr_{11}X$: A = Cs, Rb; Tr = Ga, In, Tl; X. = Cl, Br, I. *Inorg. Chem.* **1997**, *36*, 6045–6049. [CrossRef] [PubMed]

5. Kauzlarich, S.M.; Brown, S.R.; Snyder, G.J. Zintl phases for thermoelectric devices. *Dalton Trans.* **2007**, 2099–2107. [CrossRef] [PubMed]

6. Wade, K. Structural and Bonding Patterns in Cluster Chemistry. In *Advances in Inorganic Chemistry and Radiochemistry*; Emeléus, H.J., Sharpe, A.G., Eds.; Academic Press: Cambridge, MA, USA, 1976; pp. 1–66.

7. Ellinger, F.H.; Zachariasen, W.H. The crystal structures of $PuGa_4$ and $PuGa_6$. *Acta Crystallogr.* **1965**, *19*, 281–283. [CrossRef]

8. Curro, N.J.; Caldwell, T.; Bauer, E.D.; Morales, L.A.; Graf, M.J.; Bang, Y.; Balatsky, A.V.; Thompson, J.D.; Sarrao, J.L. Unconventional superconductivity in $PuCoGa_5$. *Nature* **2005**, *434*, 622–625. [CrossRef] [PubMed]

9. Neha, P.; Sivaprakash, P.; Ishigaki, K.; Kalaiselvan, G.; Manikandan, K.; Dhaka, R.S.; Uwatoko, Y.; Arumugam, S.; Patnaik, S. Nuanced superconductivity in endohedral gallide Mo_8Ga_{41}. *Mater. Res. Express* **2018**, *6*, 016002. [CrossRef]

10. Tillard, M.; Belin, C. Investigation in the Ga-rich side of the Mn–Ga system: Synthesis and crystal structure of $MnGa_4$ and $MnGa_{5-x}$ (x ~ 0.15). *Intermetallics* **2012**, *29*, 147–154. [CrossRef]

11. Shibayama, T.; Nohara, M.; Aruga Katori, H.; Okamoto, Y.; Hiroi, Z.; Takagi, H. Superconductivity in Rh_2Ga_9 and Ir_2Ga_9 without Inversion Symmetry. *J. Phys. Soc. Jpn.* **2007**, *76*, 073708. [CrossRef]

12. Belgacem-Bouzida, A.; Djaballah, Y.; Notin, M. Calorimetric measurement of the intermetallic compounds Cr_3Ga and $CrGa_4$ and thermodynamic assessment of the (Cr–Ga) system. *J. Alloys Compd.* **2005**, *397*, 155–160. [CrossRef]

13. Yannello, V.J.; Kilduff, B.J.; Fredrickson, D.C. Isolobal Analogies in Intermetallics: The Reversed Approximation MO Approach and Applications to $CrGa_4$- and Ir_3Ge_7-Type Phases. *Inorg. Chem.* **2014**, *53*, 2730–2741. [CrossRef] [PubMed]

14. Xie, W.; Luo, H.; Phelan, B.F.; Klimczuk, T.; Cevallos, F.A.; Cava, R.J. Endohedral gallide cluster superconductors and superconductivity in ReGa5. *Proc. Natl. Acad. Sci. USA* **2015**, *112*, E7048–E7054. [CrossRef] [PubMed]

15. Dinnebier, R.E.; Billinge, S.J.L. Chapter 1. Principles of Powder Diffraction. In *Powder Diffraction*; Dinnebier, R.E., Billinge, S.J.L., Eds.; Royal Society of Chemistry: Cambridge, MA, USA, 2008; pp. 1–19.

16. Rodríguez-Carvajal, J. *An Introduction to the Program FullProf 2000*; Laboratoire Leon Brillouin (CEA-CNRS): Saclay, Paris, France, 2001.

17. Sheldrick, G.M. Crystal structure refinement with SHELXL. *Acta Crystallogr. C Struct. Chem.* **2015**, *71*, 3–8. [CrossRef] [PubMed]

18. Sheldrick, G.M. SHELXT—Integrated space-group and crystal-structure determination. *Acta Crystallogr. A Found. Adv.* **2015**, *71*, 3–8. [CrossRef] [PubMed]

19. Andersen, O.K.; Jepsen, O. Explicit, First-Principles Tight-Binding Theory. *Phys. Rev. Lett.* **1984**, *53*, 2571–2574. [CrossRef]

20. Krier, G.; Jepsen, O.; Burkhardt, A.; Andersen, O. *The TB-LMTO-ASA Program*; Max-Planck-Institut fur Festkoorperforschung: Stuttgart, Germany, 1995.

21. Deringer, V.L.; Tchougréeff, A.L.; Dronskowski, R. Crystal Orbital Hamilton Population (COHP) Analysis as Projected from Plane-Wave Basis Sets. *J. Phys. Chem. A* **2011**, *115*, 5461–5466. [CrossRef] [PubMed]

22. Andersen, O.K. Linear methods in band theory. *Phys. Rev. B* **1975**, *12*, 3060–3083. [CrossRef]

23. Lambrecht, W.R.L.; Andersen, O.K. Minimal basis sets in the linear muffin-tin orbital method: Application to the diamond-structure crystals C, Si, and Ge. *Phys. Rev. B* **1986**, *34*, 2439–2449. [CrossRef] [PubMed]

24. Grin, Y.; Wedig, U.; Wagner, F.; von Schnering, H.G.; Savin, A. The analysis of "empty space" in the PdGa$_5$ structure. *J. Alloys Compd.* **1997**, *255*, 203–208. [CrossRef]

25. Srivichitranond, L.C.; Seibel, E.M.; Xie, W.; Sobczak, Z.; Klimczuk, T.; Cava, R.J. Superconductivity in a new intermetallic structure type based on endohedral Ta@Ir$_7$Ge$_4$ clusters. *Phys. Rev. B* **2017**, *95*, 174521. [CrossRef]